Br_2 and Cl_2 adsorption and etching of GaAs(110) studied by use of scanning tunneling microscopy

J. C. Patrin and J. H. Weaver
Department of Materials Science and Chemical Engineering, University of Minnesota, Minneapolis, Minnesota 55455
(Received 6 July 1993)

Scanning tunneling microscope images obtained after GaAs(110) exposure to Br_2 and Cl_2 reveal dissociative adsorption and etching at steps and terraces, depending on temperature, fluence, and flux. Exposure at 300 K produces a surface structure with halogen features localized within the rectangle formed by four surface As atoms, having (1×1) symmetry, and with halogen features localized on top of the surface As atoms. Adsorption for substrate temperatures between $\sim$400 K and $\sim$525 K results in linear chains along the substrate [001] direction. These chains coalesce with mixed (2×1) and $c(2\times2)$ domains. Exposure at 625 K produces volatile Br and Cl products and etching is manifest by single-layer etch pits. Longer exposures at the same flux at 625 K yield a steady-state condition in which five layers are exposed. Etching at 725 K is dominated by single-height-step retreat and triangular double-layer etch pit formation on extended terraces. The nucleation density of double-layer etch pits can be increased and single-height-step retreat can be inhibited at 725 K by increasing the Br_2 or Cl_2 flux.

I. INTRODUCTION

The widespread use of halogens in semiconductor dry processing makes it important to understand the fundamental mechanisms of etching and the interplay between kinetics and thermodynamics.[1] While there has been a wide range of studies of Si etching,[1] there have been fewer for GaAs (Refs. 2–16) and the other compound semiconductors. For GaAs, experimental investigations of the interaction with Cl have concentrated on the volatile etch products[2–8] and the effects of simultaneous electron or ion impact[4,8] and photon irradiation[9] during etching. Cl_2 has been shown to chemisorb dissociatively on GaAs(110) at 300 K to produce a saturated layer that passivates the surface.[8–12] Low-energy electron diffraction (LEED) results for saturated Cl-GaAs(110) have revealed a (1×1) pattern against an appreciable background at 300 K.[9,11] Early photoemission results suggested that Cl bonds exclusively to surface As atoms at 300 K (Refs. 10 and 11) but Troost *et al.*[12] suggested that Cl also bonds to surface Ga atoms. For Br-GaAs(110), the photoemission work by Gu *et al.*[13] showed two core-level features for Br and changes in both the Ga and As surface core-level signatures that led them to favor bonding to both Ga and As. For F-GaAs, the core-level photoemission results of McLean, Terminello, and McFeely[15] also indicated F bonding to both Ga and As surface atoms. Hence, studies to date have suggested common characteristics but also intriguing differences for these three halogens.

In this paper, we focus first on the dissociative adsorption of Cl_2 and Br_2 on GaAs(110). Using scanning tunneling microscopy (STM), we demonstrate that exposure to both halogens produces adsorption geometries that change with exposure and temperature and that bonding is more complex than previously thought. We then investigate surface morphologies following etching when the substrate temperature, the halogen flux, and the halogen fluence are varied independently. In the latter experiments, particular emphasis was placed on discerning competitive pathways for terrace etching and the role of surface steps. These results show the interplay between kinetics and thermodynamics, as for the inverse process of overlayer growth, and they suggest that the processing parameters can be adjusted to give different nanoscale etching profiles.

II. EXPERIMENT

The measurements discussed here were conducted in an ultrahigh-vacuum chamber containing a Park Scientific Instruments scanning tunneling microscope. The base pressure of the system was $\sim6\times10^{-11}$ Torr. Mirrorlike GaAs(110) surfaces were prepared by cleaving posts that were Zn-doped at 1×10^{18} and 1×10^{19} cm^{-3}. Electrochemically etched tungsten tips were cleaned by *in situ* electron bombardment. The STM length scales were calibrated in the lateral direction with the substrate lattice and in the z direction with single- and double-height GaAs(110) steps. The images were acquired at 300 K in the constant current mode with tunneling currents of 100–200 pA and bias voltages of $\pm(1.5–3)$ V. The images are displayed with the substrate $[1\bar{1}0]$ direction oriented approximately 135° from the $+x$ axis unless otherwise specified. They are not corrected for drift and this accounts for some skewing of the images.

Halogen molecules were produced by electrochemical cells built following the design described by Spencer *et al.*[17] These ultrahigh vacuum compatible solid-state cells contain a AgBr or AgCl pellet doped with $CdBr_2$ or $CdCl_2$ housed in a Pyrex tube. When a voltage is applied, the halogen ions diffuse to one end, a Pt electrode, where they desorb as Br_2 or Cl_2. Exposures were then calibrated by Faraday's first law that relates the current through the cell to the amount of released gas. The currents used here were 6 or 60 μA. Exposures are quoted in terms of the products of the current time, mA s. The source was $\sim$2 cm from the GaAs(110) surface with a direct line of

sight from the Pt grid. Under operating conditions of 6 μA, the source evolves $\sim 1.8\times10^{13}$ molecules per second. We note that the flux incident upon the sample was specific to the experimental geometry. Moreover, the sticking coefficient depends on the conditions and temperature of the surface. The sample temperature was monitored using an optical pyrometer. After exposure, the sample was cooled rapidly to room temperature and the measurements were initiated within ~ 60 min.

III. RESULTS AND DISCUSSION

A. Br and Cl adsorption on GaAs(110), 300–575 K

Molecular bromine and chlorine adsorption on GaAs(110) is dissociative. For Br-GaAs(110), recent photoemission studies[13] revealed two components in the Br $3d$ core-level emission after adsorption at 300 K that were interpreted in terms of bonding to Ga and As surface atoms. For Cl-GaAs (110), there has been disagreement as to whether the adatoms bond only to As (Refs. 10 and 11) or to both Ga and As (Ref. 12). Figures 1(a)–1(d) show the GaAs(110) surface after Br_2 exposures at temperatures that facilitate ordering but yield minimal etching. Figures 2(a) and 2(b) show corresponding results

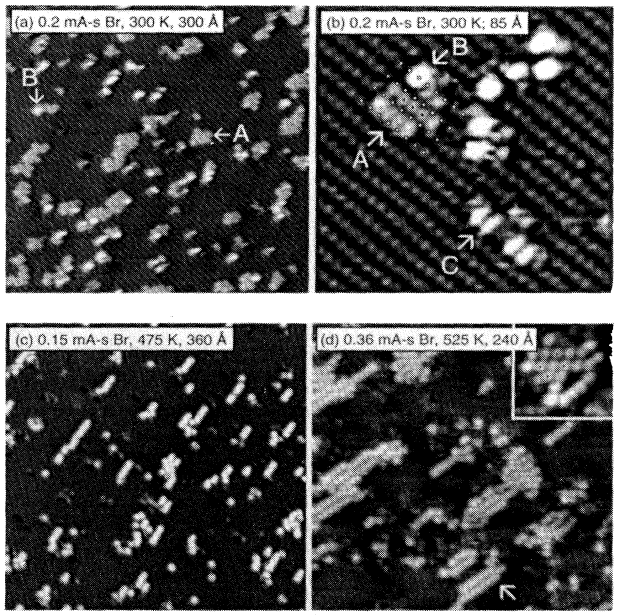

FIG. 1. (a) Adsorption structures for Br on GaAs(110) at 300 K showing A-type islands and B-type defects within the islands. (b) Curvature-enhanced image showing that the A features are localized within the rectangle formed by four As atoms. The black dots represent maxima of A-type features and the white dots represent the As atoms. The B-type features are above As atoms. (c) Image obtained after Br_2 exposure at 475 K showing linear chains elongated along [001]. (The image is not corrected for drift.) (d) Image demonstrating the coalescence of one-dimensional (1D) chains into two-dimensional (2D) islands. The arrow points to a region with (2×1) symmetry. The inset shows a region with $c(2\times2)$ symmetry as highlighted by four black dots.

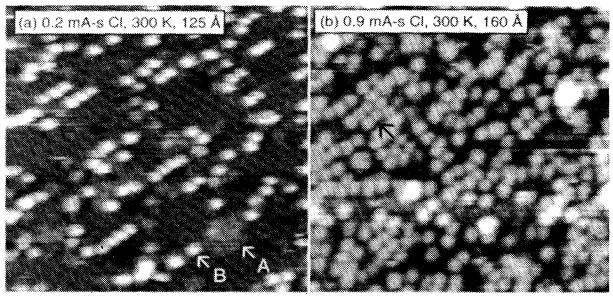

FIG. 2. (a) A 125×125-Å^2 image after a 0.2-mA s exposure to Cl_2 at 300 K showing A- and B-type adsorption features, as for Br. (b) A 160×160-Å^2 image for the nearly saturated Cl-GaAs(110) surface. The arrow highlights a B-type region with local (2×1) symmetry.

for Cl_2-exposed GaAs(110), and Fig. 3 depicts the chemisorption structure deduced from the STM images (rotated 45° relative to the STM images).

The images of Figs. 1(a) and 1(b) were obtained after exposure to 0.2 mA s of Br_2 at 300 K. Two distinct Br-induced features are clearly evident, labeled A and B. The A features form 1–1.2-Å-high islands where the spacing between features is 5.6 Å along [001] and 4 Å along $[1\bar{1}0]$. They appear within the rectangle defined by four As surface atoms, resulting in a (1×1) structure that would be saturated at 4.43×10^{14} atoms cm^{-2}, as depicted at the left of Fig. 3. (We note that the exact position within the rectangle is not known since STM images reflect charge distributions,[18] not necessarily nuclear positions.) The features labeled B are 2.1–2.3 Å high, relative to the substrate, when measured with negative sample bias and ~ 2.6 Å when measured with positive sample bias. At low exposure at 300 K, the B features appear as defects within A-type islands, centered above surface As atoms. Two such defects are sketched in the island at the left of Fig. 3. A third type of feature, labeled C, is also

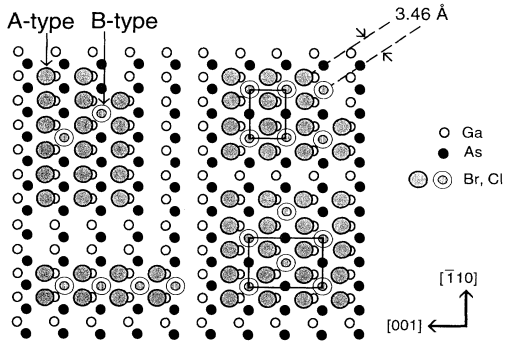

FIG. 3. Model depicting the adsorption sites for Br and Cl on GaAs(110). The A-type islands apparent at 300 K and low exposure have halogen-induced features within the rectangle formed by four As atoms. The B-type features are located above the As atoms. Heating produces chain structures derived of A and B features elongated along [001], as shown at bottom left. More extended exposure produces coalesced chains, as depicted at the right for the (2×1) and $c(2\times2)$ structures.

observed, though less frequently. These are 1.5–1.6 Å high and are spaced ~4 Å apart along [1$\bar{1}$0]. They are located above As rows but between As atoms. The C features appear in pairs along the edges of the A-type islands. The B and C features are higher than the A-type features around them and they obscure their neighbors in the STM images. No features equivalent to these were observed for the clean surface.

Figure 1(c) shows that exposure at 475 K to 0.15 mA s of Br_2 enhances chain formation with elongation along [001], as depicted at the bottom left of Fig. 3. [Figure 1(c) exhibits drift such that [1$\bar{1}$0] is oriented more than 135° from the x axis.] Dual-bias images demonstrate that the maxima of the B-type features are located over As rows for both biases, as when such features appear as minority species in A islands. Under these conditions, we found no evidence of islands derived only from A-type features. Likewise, annealing the surface characterized by Fig. 1(a) to 400 K eliminated the all-A islands and produced chain structures.

Figure 1(d) shows that the chains coalesce and produce islands with (2×1) symmetry after exposure at 525 K to 0.36 mA s of Br_2. Such coalescence is also apparent after continued exposure at low temperature, but the degree of ordering is lower. The arrow identifies a (2×1) domain. The inset shows a region of local $c(2\times2)$ symmetry that results when a column of B-type features shifts by 4 Å along [1$\bar{1}$0], as depicted in the bottom right of Fig. 3. Inspection of the image of Fig. 1(d) shows that imperfect ordering is commonplace under these conditions. Hence, LEED images would reflect the order of the overlayer but the background would be significant, as observed.[9,11]

Chemisorption results similar to those for Br-GaAs(110) were obtained for Cl-GaAs(110). Although the quality of the image of Fig. 2(a) is not as good as that for Br-GaAs, the features labeled A constitute an island elevated 0.7–0.8 Å relative to the substrate. The rows within the A-type islands are located between As rows. There are also B-type features that appear about 1.5–1.7 Å high for a negative sample bias (~2 Å for positive bias) and are located above As atoms, as for Br-GaAs. Comparison suggests more B-type features and more linear alignment along [001] for Cl-GaAs than for Br-GaAs for equivalent exposures at 300 K. Chain elongation was even more pronounced for exposure at 475 K. The adsorption sites were less ordered than those of Fig. 1(d) for higher Cl exposures at 300 K but there were B-type regions of local (2×1) symmetry, as identified by the arrow in Fig. 2(b). Again, ordering could be increased by raising the temperature during exposure. Comparison indicates analogous adsorption behavior for Cl and Br on GaAs(110) with the same locations for the A and B features, similar chain formation, and ordering near saturation. We found no evidence that would suggest fundamental differences in surface bonding for Br and Cl.

The adsorption geometries depicted in Fig. 3 describe the experimental results. The low coverage results are represented by A-type islands, often with B-type additions, as sketched at the upper left of Fig. 3. The nearest-neighbor distance between the A- and B-type features is 3.46 Å along the diagonal of the GaAs surface unit cell. This is large compared to a bond length of 2.29 Å for molecular Br_2. The A-type features are located between four As atoms and close to a Ga atom in this low-density structure. The B-type additions are located over As atoms. The conversion of A-type islands into chain structures is depicted in the lower left of Fig. 3. In this case, the higher B-type features dominate the STM images. Increased Br or Cl exposure leads to the chain coalescence depicted for the (2×1) region in the upper right of Fig. 3. An offset of one B-type column along [1$\bar{1}$0] produces a $c(2\times2)$ structure.

The Br- and Cl-induced features observed in Fig. 1(a) are mobile at 300 K under our measuring conditions. In particular, isolated B-type features could move against the background of the A-type islands, A-type features could be added to island perimeters, and features comprising the perimeter could rearrange. Likewise, a sudden increase in the bias to ~4 V could create a mound beneath the tip, suggesting that the electric field might play a role in halogen diffusion, as for highly polarizable Cs atoms on GaAs(110).[19] Glitches often occurred when scanning over halogen features, indicating that atoms were "moving" under the tip.

The geometries depicted in Fig. 3 are not what we might have expected based on photoemission results obtained after Br_2 exposure at 300 K. In particular, two Br 3d core-level doublets of nearly equal intensity were observed.[13] This suggested bonding to Ga sites and to As sites in about equal proportion. While these distinct features might correspond to the A- and B-type features observed with STM, the core-level intensities do not agree with the observation of A-dominated adsorption sites at 300 K. Moreover, heating to 430 K reduced the relative intensity of the shallower Br 3d feature, i.e., the one attributed to As bonding. In contrast, the STM images showed an increase in the number of B features relative to A features. We suggest, therefore, that the photoemission spectra reveal energy shifts that are more complicated in origin than previously thought, with more extensive substrate-mediated effects. The development of a chain along [001] points to substrate involvement, as for Cs chains on GaAs(110) and InSb(110),[19,20] although the mechanism for chain formation remains elusive.

Theoretical treatments of surface bonding using a linear-combination-of-atomic-orbitals approach[12] focused on the energies of the bonding, nonbonding, and antibonding levels for Ga-Cl and As-Cl "surface molecules." They compared their calculations to photoemission observations and concluded that Cl bonded to both Ga and As. In contrast, Margaritondo *et al.*,[10] using empirical tight-binding methods and photoemission, concluded that Cl bonded only to surface As atoms. We find no support for the latter conclusion. While there have not yet been calculations to determine the minimum energy structures for halogens on GaAs(110), we suggest that the results would be very informative.

B. Terrace etching, $T < 575$ K

Inspection of Figs. 1(c) and 2(a) shows an increase in the number density of dark objects relative to the starting

surfaces. Dual-bias images indicate that the dark objects are derived from Ga-As pair vacancies and to single-atom vacancies. These vacancies remain isolated and small in size under the conditions of their creation by halogen etching, implying minimal vacancy diffusion. This result differs from what has been observed for Si vacancies created on Si(100) by ion-beam irradiation at 725 K because the Si vacancies were able to diffuse to B-type Si step edges.[21]

Extended surface modification could be induced by increased halogen exposures, even at temperatures of only 475 K.[22] In particular, exposure to 1.8 mA s of Br_2 at 475 K [12 times the fluence of Fig. 1(c) but at the same temperature and flux] resulted in a surface with mixed (2×1) and $c(2\times2)$ Br structures but with two layers offset by 2 Å. This indicates surface etching that exposes the subsurface GaAs layer. On this near-surface layer, the Br adsorption sites are equivalent to those for the unetched layer. These lower-level islands were irregular in shape and size. Within them, there were also small dark areas that indicated second-layer etching. (Such etching is discussed in more detail in Sec. III C.)

To investigate the surface morphology produced by etching a partially covered GaAs(110) surface, we heated the sample represented by Fig. 1(d) for 10 min at 575 K. Before heating, the surface showed Br-derived chain structures elongated along [001]. After heating, ~20% of the first layer was removed but the etch pattern would not mirror the chemisorption chain geometry. Instead, the etch patterns were irregular and one layer deep.

C. Terrace etching, 625–825 K

One of the goals of this study was to investigate etching under conditions where the flux, fluence, and temperature were varied independently. Figure 4 summarizes measurements where the fluence and the temperature were adjusted independently but the flux was fixed. Under these conditions, the flux was relatively low because operation of the source at 6 μA implied the evolution of 1.8×10^{13} Br_2 molecules per second. Again, the sticking coefficient depends on temperature and surface conditions and there are no quantitative measures of those parameters.

Figure 4(a) shows an image with irregularly shaped etch pits obtained after exposure at 625 K to 0.36 mA s of Br_2. Most are one layer deep, denoted single height (SH) henceforth, although a few show second-layer vacancy formation, highlighted by arrows. The etch pits are bounded by SH $[1\bar{1}0]$ and [001] steps but these steps have a large number of kinks, as shown in the inset for the etch pit enclosed by the box. While such irregular structures are less than ideal, they offer a range of accommodation and etching sites for Br atoms. The large etched regions of Fig. 4(a) probably represent the coalescence of smaller etch pits.

Figure 4(b) shows an image obtained after exposure to a Br_2 fluence five times greater than in Fig. 4(a) at the same temperature. Again, the islands and pits are irregular in overall shape but they are generally bounded by kinked $[1\bar{1}0]$ and [001] steps. In this case, five different

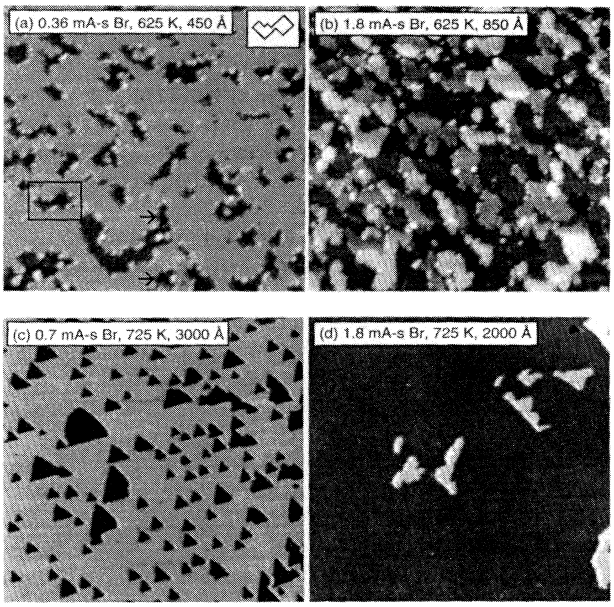

FIG. 4. (a) A 450×450-Å^2-image after exposure to 0.36 mA s of Br_2 at 625 K showing etch pits that are one layer deep and bounded by SH $[1\bar{1}0]$ and [001] steps. The inset shows the outline of the SH etch pit highlighted by the box. The arrows identify areas where second-layer pitting has occurred. (b) An 850×850-Å^2 image after a 1.8-mA s Br_2 exposure at 625 K showing five different substrate layers showing simultaneous multilayer etching. The rms surface roughness is ~2 Å. (c) A 3000×3000-Å^2 image of a typical area on an extended terrace after exposure to 0.7 mA s of Br_2 at 725 K. The image shows triangular double-layer etch pits with {111} microfacets. (d) A 2000×2000-Å^2 image after a 1.8-mA s exposure to Br_2 at 725 K. Two layers have been removed from most of the surface. The remnants of this bilayer are evident as white islands.

substrate layers are evident. Analysis reveals a root-mean-square roughness of 2 Å, implying that ~70% of the surface falls within ±1 layer of the average height. Subsequent Br exposure led to continued etching but the overall surface morphology did not change appreciably and the rms surface roughness remained at ~2 Å. The layer irregularity suggests that Ga and As mobility around the perimeter of an island or vacancy is not large. Also apparent in Figs. 4(a) and 4(b) are bright spots around the edges of the islands or etch pits. Such features were less frequently observed at higher temperature. We speculate that they are residual surface species liberated by etching.

Figure 4(c) shows a typical region of a terrace after exposure at 100° higher temperature, 725 K, with 0.7 mA s of Br_2. Comparison shows that a new etching pathway was dominant at this temperature and the surface morphology was very different. In particular, the etch pits that were formed were two layers deep (4 Å). These double-height etch pits, henceforth denoted DH, had triangular shapes that indicated preferred etching directions. The DH etch pits are particularly well defined in Fig. 4(c) and several have coalesced. The triangular boundaries are defined by an As-terminated $[1\bar{1}0]$ step

and somewhat more irregular [$\bar{1}12$] and [$1\bar{1}2$] steps. The atomic arrangements at these DH steps resemble {111} microfacets with reconstructions that are discussed in the context of Fig. 5 below.

Figure 4(d) shows an image obtained after exposure to the same amount of Br_2 as in Fig. 4(b) but at higher temperature. The islands are 4 Å (two layers) above the surrounding terraces and most are bounded by DH {111} facets. Comparison to Fig. 4(c) shows that the effect of additional Br_2 exposure was to allow etch-pit coalescence and the removal of a bilayer from the GaAs surface. Under these conditions, there is little etching into the exposed terrace. This indicates that etching at the DH steps was favored relative to etch-pit creation on a terrace. Clearly, the etching conditions were very different from those of Fig. 4(b) where five irregular layers were exposed by the same halogen exposure but at lower temperature.

The results of Fig. 4 emphasize the etching counterpart to what is observed during overlayer growth.[23] In particular, both etching and growth involve adatom condensation onto a terrace with subsequent movement that is controlled by the temperature and the activation energies for diffusion. During growth, if diffusion to a step edge is possible (a kinetic consideration) and accommodation is favored (a thermodynamic consideration), then the overlayer will grow by step flow. Deposition under conditions of insufficient kinetics promotes adatom island nucleation on the terrace, resulting in the formation of an $(n+1)$ layer prior to completion of the nth layer, i.e., simultaneous multilayer growth. From Fig. 4(a), we see that exposure to an etching species at 625 K leads to vacancy creation and lateral growth but equilibrium shapes are not achieved. Increased fluence results in multilayer etching profiles as shown by Fig. 4(b), as conditions favorable to single-layer pitting are met on the terraces. Clearly, surface diffusion is not sufficient at 625 K to allow layer-by-layer etching or to allow the etch pits to adopt equilibrium shapes. At 725 K, however, etch pits with distinct equilibrium shapes are favored and the etching of the surface follows a bilayer-by-bilayer removal pattern.

D. Single-height vs double-height etch-pit formation

Figure 5 shows images obtained after exposure to Br_2 and Cl_2 under lower temperature conditions where SH terrace etching is favored and at higher temperature where DH etching prevails. These images allow inspection of the etch-pit shapes when they are very small, extending over only a few rows of the surface.

Figure 5(a) shows a terrace region after exposure to 0.37 mA s Cl_2 at 625 K. The GaAs[$1\bar{1}0$] rows run diagonally across the image, as usual. Etching at this temperature is dominated by SH substrate removal with etch pits that are defined by highly kinked [$1\bar{1}0$] and [001] steps. The bright spots near the pits are likely to be etch products that have not desorbed. These bright spots exhibit no apparent periodicity. Figure 5(b) shows DH etch pits where all of the features are 4 Å (two layers) deep. Although feature I is a complex, the area at the left is triangular and extends across seven rows. Features II and III are also irregular and extend over two to four rows. The better-defined edge corresponds to an As-terminated DH [$1\bar{1}0$] step, as highlighted by an arrow for feature II. The opposite side shows features that are spaced 8 Å apart along [$1\bar{1}0$] and appear to project into the pit, as highlighted by the arrow for feature III. Apparently, a readily-formed DH vacancy row is formed and etching occurs perpendicular to this row to establish a triangular shape, even when the pit is very small. Several such nascent structures are apparent in Fig. 5(b). There is no indication that SH etching is a necessary precursor to DH etching. Exposure to Br_2 at somewhat higher fluence at 725 K produces equivalent DH triangular etch pits, as is evident in Fig 5(c) for a feature that extends across approximately ten rows and is bounded by [$1\bar{1}0$] and imperfect [$1\bar{1}2$] and [$\bar{1}12$] rows. Continued exposure results in large triangular features such as those illustrated in Fig. 4(c). Minimal etching occurs into the newly exposed region, implying much-favored lateral etching.

Figure 5(d) focuses on the reconstruction on an As-

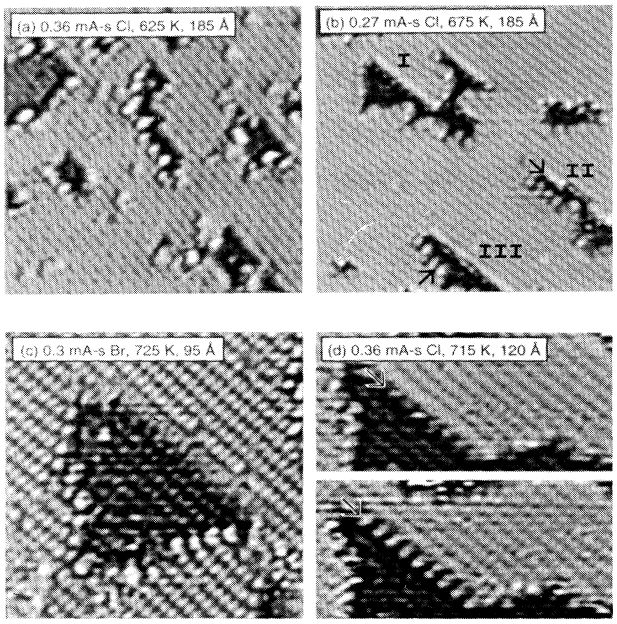

FIG. 5. (a) A 185×185-Å^2 image after Cl_2 exposure at 625 K. At this temperature, etching is initiated by SH pits composed of [$1\bar{1}0$] and [001] steps. (b) A 185×185-Å^2 image after exposure to Cl_2 at 675 K. The etch pits are all two layers deep (4 Å) and show the onset of triangular pit formation as in I. The arrow by II points to the As-terminated [$1\bar{1}0$]-step. The arrow by III draws attention to a two-times periodicity in the step reconstruction. The reconstruction is also evident in I and II on the straight [$1\bar{1}0$] boundaries. (c) Atomic resolution image after exposure to Br at 725 K showing a double height (DH) triangular etch pit composed of [$\bar{1}12$], [$1\bar{1}2$], and [$1\bar{1}0$] steps. These DH steps form {111} microfacets. (d) STM image obtained with negative and positive sample bias (top and bottom) after Cl_2 exposure at 715 K. The image shows a double-layer etch pit at the top and middle of the figure. The {111} microfacet at the As-terminated [110] step has a two-times periodicity in the [$1\bar{1}0$] direction as highlighted with an arrow for both biases.

terminated [1$\bar{1}$0] step produced by exposure to Cl_2 at 715 K. The upper and lower panels were obtained with negative and positive sample bias, respectively. In positive bias, there are features that are clearly evident along the step. They are less apparent for negative sample bias. They are separated by 8 Å along [1$\bar{1}$0] defining a two-times periodicity. An example of the reconstruction for As-terminated steps is seen in Fig. 5(d) and, less evidently, in feature I of Fig. 5(b). The arrow of feature III in 5(b) identifies regions of the two-times reconstruction for Ga-terminated steps. Overlaying the images obtained with positive and negative bias demonstrates that the maxima in the two-times reconstruction are located in the same position. Since it is not possible to associate a maximum in the charge density with Ga or As lattice sites of the clean surface, we cannot offer a model of the detailed structure of the DH step reconstruction. We do note, however, that two-times periodicity of these {111} microfacets bears a striking resemblance to what has been reported for reconstructed GaAs($\bar{1}\bar{1}\bar{1}$) and (111) surfaces.[24,25] In particular, double periodicity has been observed along [1$\bar{1}$0], effects attributed to the formation of As adatom trimers for GaAs($\bar{1}\bar{1}\bar{1}$) or missing Ga atoms for GaAs(111). Here, the two-times reconstructions may play an important role in determining the etching profiles for GaAs(110) since they are characteristic of the dominant DH etch-pit boundaries.

E. GaAs(110) step etching

Cleaved GaAs(110) surfaces are characterized by large defect-free terraces, at least under ideal conditions. Even for those surfaces, however, there are also steps that tend to be aligned along ⟨110⟩, ⟨001⟩, and ⟨112⟩. Their presence makes it possible to investigate competition between etching at steps and pit formation on the nearby terraces. As for the analogous case of epitaxial growth,[23] we find depleted zones free of etch pits near certain steps. These results reflect a balance between energies and kinetics.

Figure 6(a) shows a portion of a SH [$\bar{1}$12] step after exposure to 0.36 mA s of Cl_2 at 625 K. Under these conditions, the step edge is very ragged with rows of material removed along [1$\bar{1}$0]. There are irregular SH etch pits on the terraces that are again bounded by [1$\bar{1}$0] steps and resemble those produced by Br exposure at the same temperature, [Fig. 4(a)]. Significantly, the number of etch pits near the step is nearly the same as on the open terrace, indicting that the step does not act as a sink for Cl in this temperature regime. Such step plus terrace etching is analogous to what is observed during growth under kinetic conditions that prevent diffusion to the step edge.

Figure 6(b) shows a SH [1$\bar{1}$0] step that crosses the image at the upper right and another that intersects a SH [1$\bar{1}$2] step in the center. Exposure to Br_2 at this temperature produces triangular DH etch pits on the terraces, as in Fig. 4(c), but they are less regular because of the lower temperature. The SH [1$\bar{1}$0] cleavage steps are reasonably straight but there are also kinks and occasional regions that indicate etching into the upper or lower terrace. Near these steps, the etch-pit density is approximately the same as on the extended terraces. In contrast, the [1$\bar{1}$2] step shows significant terrace etching. In this case, the original step location is still apparent but the terraces on either side have been eroded. The extent of such erosion of the [1$\bar{1}$2] step region is clearly greater than on the terraces or near the SH [1$\bar{1}$0] steps. Near the [1$\bar{1}$2] step, the features are bounded by SH and DH [1$\bar{1}$0] terrace steps. Double-layer etching into the lower terraces establishes a triple-height step at the boundary with the upper terrace. This serves to retard etching into the upper terrace. The DH etch pits in the lower terrace again present {111} microfacets. These DH triangular depressions are larger near the original [1$\bar{1}$2] step than on the extended terrace and the number of terrace etch pits close to the [1$\bar{1}$2] step is small. This is consistent with diffusion to, and accommodation at, [1$\bar{1}$2] steps with subsequent etching into the terrace.

The difference in SH ⟨1$\bar{1}$2⟩ and ⟨1$\bar{1}$0⟩ step reactivities reflects a combination of factors. First, atoms at ⟨1$\bar{1}$0⟩ steps have one dangling bond while those at ⟨1$\bar{1}$2⟩ steps have two and, though the detailed atomic structure at the steps is now known, the increased number of dangling

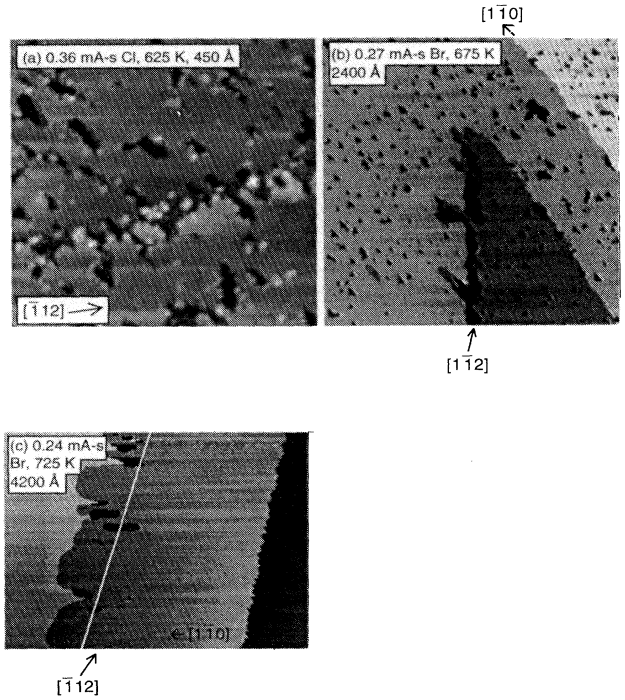

FIG. 6. (a) A 450×450-Å^2 image after Cl_2 exposure at 625 K. The image shows a [$\bar{1}$12] single-height (SH) step at the center. The etch pits on each terrace are one layer deep (2 Å) and the step shows etching along [1$\bar{1}$0]. (b) A 2400×2400-Å^2 image after Br_2 exposure at 675 K showing a [1$\bar{1}$0] step in the upper right and another that intersects a [1$\bar{1}$2] step at the center. The [1$\bar{1}$2] step has been modified substantially but the [1$\bar{1}$0] step shows little evidence of etching. (c) A 4200×3000-Å^2 image obtained after Br_2 exposure at 725 K. The white line approximates the original position of the SH step, showing retreat to the left by ~500 Å. The right portion of the image shows a DH step with local sawtoothlike structure. Note that the [1$\bar{1}$0] direction is along the x axis.

bonds should enhance etching. Second, the diffusion of Br on GaAs(110) terraces is likely to be anisotropic,[26] resulting in preferential transport along $\langle 1\bar{1}0 \rangle$ relative to $\langle 001 \rangle$. The higher Br-delivery rate to the more reactive $\langle 1\bar{1}2 \rangle$ steps can account for the observed contrast in etching.

Figure 6(c) shows a SH $[1\bar{1}2]$ step at the left and a DH $[1\bar{1}2]$ step at the right after exposure to 0.24 mA s of Br_2 at 725 K. The white line approximates the position of the original SH step. Note that it is not strictly aligned along $[1\bar{1}2]$ and this image is rotated relative to all the others presented here so that $[1\bar{1}0]$ is along the x axis, as indicated. At this temperature, etching resulted in the retreat of the SH $[1\bar{1}2]$ step by approximately 500 Å. The step is not straight, however, and large-scale deviation from linearity can be related to pinning faults created at the retreating step edge when etching occurs into the lower terrace. Figure 6(c) shows five fingers or peninsulas that extend to the right from the retreating SH $[1\bar{1}2]$ step. Each is terminated by a DH step. These peninsulas have long sides that represent SH $[1\bar{1}0]$ steps. Etching into the peninsulas, perpendicular to the zigzag chain direction, is slower than along $[1\bar{1}0]$ but it does account for their thinning and ultimate disappearance. This backcutting is responsible for the isolation of the SH etch regions near the position of the original step. The formation of rectangular etch pits in the lower terrace can be understood by noting that the DH fault creates a step that can flow along $[1\bar{1}0]$ into the lower terrace. Such patterns are clearly evident in Fig. 6(b).

The rectangular shape of the SH etch pits reflects an anisotropy in the etching rates. To quantify this, we measured the aspect ratio of the SH rectangular etch pits for Br exposures at 725 K near SH $[1\bar{1}2]$ steps and on extended terraces. Analysis shows that elongation along $[1\bar{1}0]$ was at least ~ 4.5 times that along [001].[16] This underestimates the etching anisotropy because the rectangular etch pits were created by DH fault formation, as discussed above, and growth into the DH step is retarded until the peninsula is backcut and the double step is converted to a single step. The aspect ratio of the rectangular etch pits increases with increasing substrate temperature as the diffusion length increases.

The right side of Fig. 6(c) shows a DH $[1\bar{1}2]$ cleavage step. Imaging of this step over a total length of about 10 000 Å indicated that it was straight in overall appearance but locally was derived from a sawtooth structure. Inspection shows that the edges of the sawtooth are again DH $[1\bar{1}0]$ and $[\bar{1}12]$ steps, as in the triangular pits of Fig. 4(c).

An indication of the different Br accommodation coefficients of SH and DH $[\bar{1}12]$ steps can be found by determining the density of pits on the adjacent terrace. Measurements made 500 Å on either side of a given step show that the defect density near a DH step is nearly the same as on extended terraces but is only about half as large near SH steps. Hence, these single-height steps act as sinks for Br atoms and are preferred reaction sites.

Cleaving GaAs(110) also creates SH $\langle 001 \rangle$ in addition to the SH $\langle 112 \rangle$ and SH $\langle 110 \rangle$ steps discussed above. STM images of these steps after Br_2 or Cl_2 exposure show step flow analogous to that evident in Figs. 6(b) and 6(c) for SH $\langle 112 \rangle$ steps. In particular, the step retreats along $[1\bar{1}0]$ as atoms are removed along the zigzag chain direction. As for Fig. 6(c), faults are created in the lower terrace and these pin the upper terrace, resulting in the formation of peninsulalike structures and step flow into the lower terrace.

F. Br-GaAs(110) flux-dependent etching

To investigate how the surface morphology changes as a function of the concentration of halogen atoms present at any given time, we increased the flux by a factor of 10 compared to the above. Figure 7(a) shows a 3500×3500-A^2 image obtained after 0.6-mA s Br_2 exposure at 725 K (60-μA cell current) to emphasize the etching behavior near a SH $[1\bar{1}2]$ surface step where multiple layers with rectangular etch pits were produced. Comparison to Fig. 6(c) demonstrates that the increase in flux accelerated SH $[1\bar{1}2]$ retreat but also facilitated the formation of DH faults. Inspection of the features extending from the terrace on the left shows that much of the terrace edge is terminated by such DH faults. In turn, flow of the newly created $[1\bar{1}2]$ step away from the fault was ultimately impeded by another fault. As a result, the final surface shows significant interdigitation. Away from the original step region, we again see triangular DH etch pits. A simple estimate of the amount of material removed from the terrace by triangular DH etch-pit formation and growth from the optical step-by-step flow indicates that the latter is much more favorable. The tenfold increase in flux and 2.5-times increase in fluence compared to Fig. 6(c) created conditions that led to a rougher surface.

In another portion of the surface, we observed a step that was originally five layers high (10 Å) that ran along $[1\bar{1}2]$. We found that the triangular DH etch-pit density decreases with approach toward the multiple step from either side, an effect also evident in Fig. 7(a). Hence, multiple-height steps also act as sinks for Br. In this case, however, etching was very evident at the top of the step but little etching into the lower terrace was detected.

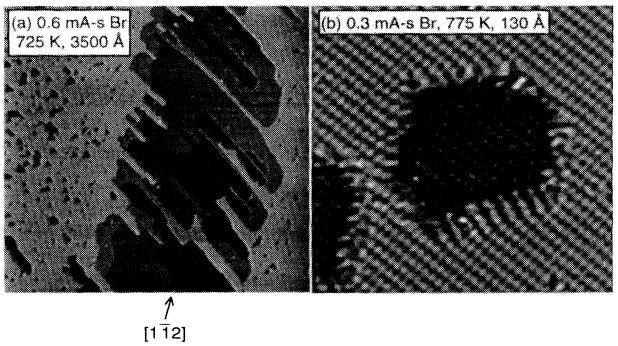

FIG. 7. (a) A 3500×3500-Å image after a Br_2 exposure at 725 K to ten times the flux of the earlier images. The left part is one layer higher than the right. The increase of Br on the surface facilitates etching into the terraces and produces multilayer exposure near the original step. (b) An atomic resolution image of a typical DH etch pit obtained after Br_2 exposure at 775 K. The etch pit is composed of six {111} microfacets.

This suggests that Br incident from the lower terrace was easily transported to the step top (locally moving along $[1\bar{1}0]$) when successive layers were etched.

An increase in the temperature to 775 K (60-μA cell current) resulted in DH etch pits that were no longer triangular in overall appearance but were bounded by the same type of DH $\langle 1\bar{1}2\rangle$ and $\langle 1\bar{1}0\rangle$ steps as for Fig 5(c), although with a greater kink density. The varied etch-pit shapes are probably the consequence of pit coalescence. There were also large elongated structures, like that seen in the lower left in Fig. 7(a), that have regions that are one, two, and three layers deeper than the surrounding terrace. Under these etching conditions with much-enhanced local Br concentration, it is apparent that single-layer etching is again possible but also that the large number of DH etch pits prevent extensive SH step flow.

Finally, the high-resolution image of Fig. 7(b) shows that the DH etch pits produced at 775 K exhibit sixfold, rather than threefold, symmetry. Three of the sides are still $\{111\}$ facets with DH $[1\bar{1}2]$, $[\bar{1}12]$, and As-terminated $[1\bar{1}0]$ steps. We suggest that the change implies that etching of Ga-terminated $\{111\}$ facets is facilitated at higher temperatures. By inference, we suggest that three original DH $\{111\}$ facets are all As terminated and the three facets exposed at higher temperature and flux are Ga terminated. We note that Furuhata *et al.*[27] observed that the etch rate for $\{111\}$ Ga- and As-terminated planes becomes nearly equal for Cl_2 dry etching of GaAs above $\sim$725 K, consistent with our observation of hexagonal etch pits.

IV. SUMMARY

Figure 8 summarizes the results obtained after GaAs(110) was exposed to Br_2 and Cl_2 at the temperatures indicated under conditions of low flux. STM results show that halogen adsorption is dissociative and that both Br and Cl exhibit (1×1) adsorption structures for low-density A-type islands. Exposure at 400 K produces chains that are elongated along [001]. These chains coalesce into locally ordered regions of $(2\times1)/c(2\times2)$ symmetry.

The observed etching behavior of GaAs(110) is equivalent for Br and Cl. At 625 K, etching begins by the formation of SH pits that are irregular in overall appearance but are bounded by kinked $[1\bar{1}0]$ and [001] steps. Continued exposure at 625 K produces a steady-state surface morphology that exposes approximately five different layers. This simultaneous multilayer etching reflects insufficient kinetics for layer-by-layer removal, paralleling simultaneous multilayer growth. An increase in temperature to $\sim$675 K changes the etch pattern as DH triangular etch pits are formed. These are bounded by $[1\bar{1}0]$, $[1\bar{1}2]$, and $[\bar{1}12]$ steps and expose $\{111\}$ microfacets.

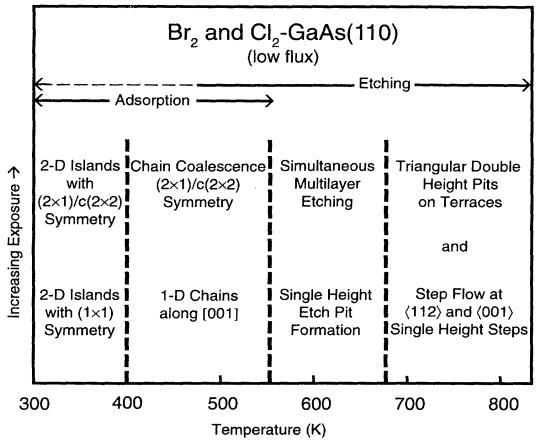

FIG. 8. Schematic summary of halogen interaction with GaAs(110) under conditions of low flux at temperatures indicated. The boundaries between the different phases are not intended to be sharp. Transitions from one structure to the other are gradual and only the dominant behavior is given. At higher flux, the etching of SH steps at 725 K produces more multilayer etching and hexagonal DH etch pits replace triangular DH pits at 775 K. The dashed line at the tip implies that etching is still possible at temperatures below $\sim$475 K but occurs at a much reduced rate.

For temperatures between about 675 and 725 K, we have observed etching at SH $\langle 112\rangle$ and $\langle 001\rangle$ and minimal etching at SH $\langle 110\rangle$ steps. The result was multilayer pitting near the steps. With increased temperature, the multilayer pitting was reduced and step retreat was observed. Though reduced, fault formation did occur at the retreating step and this allowed etching along $[1\bar{1}0]$ into the lower terrace, producing rectangular SH etch pits that were pinned by double-height faults.

Under conditions corresponding to a tenfold increase in the halogen flux, we found an increase in the density of triangular DH etch pits and increased multilayer etching in the vicinity of surface SH steps. Likewise, at higher temperatures we found that the triangular etch pits were replaced by hexagonal etch pits, again exposing $\{111\}$ microfacets.

These results have shown that it is possible to vary the surface profile by controlling the temperature, flux, and fluence during etching for GaAs(110). They show the competition between kinetics and equilibrium growth such that multilayer etching is observed at lower temperature or at higher flux.

ACKNOWLEDGMENTS

This work was supported by the Office of Naval Research. The authors thank Y. Z. Li, M. Chander, F. Stepniak, and D. Rioux for discussions and assistance.

[1]See, for example, the excellent review by H. F. Winters and J. W. Coburn, Surf. Sci. Rep. **14**, 161 (1992), and references therein. See also M. Chander, Y. Z. Li, J. C. Patrin, and J. H. Weaver, Phys. Rev. B **47**, 13 035 (1993).

[2]M. Balooch, D. R. Olander, and W. J. Siekhaus, J. Vac. Sci. Technol. B **4**, 794 (1986).

[3]S. M. Mokler and P. R. Watson, Solid State Commun. **70**, 415 (1989).

[4]G. C. Tyrrell, D. Marshall, J. Beckman, and R. B. Jackman, J. Phys. Condens. Matter **3**, S179 (1991).
[5]C. L. French, W. S. Balch, and J. S. Foord, J. Phys. Condens. Matter **3**, S351 (1991).
[6]A. Ludviksson, M. Xu, and R. M. Martin, Surf. Sci. **277**, 282 (1992).
[7]S. M. Mokler, P. R. Watson, L. Ungier, and J. R. Arthur, J. Vac. Sci. Technol. **10**, 2371 (1992).
[8]L. A. DeLouise, J. Chem. Phys. **94**, 1528 (1991); Surf. Sci. **244**, L87 (1991); J. Vac. Sci. Technol. A **9**, 1732 (1991); J. Appl. Phys. **70**, 1718 (1991).
[9]V. Lieberman, G. Haase, and R. M. Osgood, Jr., J. Chem. Phys. **96**, 1590 (1992).
[10]G. Margaritondo, J. E. Rowe, C. M. Bertoni, C. Calandra, and F. Manghi, Phys. Rev. B **20**, 1538 (1979); **23**, 509 (1981).
[11]R. D. Schnell, D. Rieger, A. Bogen, K. Wendelt, and W. Steinmann, Solid State Commun. **53**, 205 (1985).
[12]D. Troost, L. Koenders, L.-Y. Fan, and W. Mönch, J. Vac. Sci. Technol. B **5**, 1119 (1987); D. Troost, H. J. Clemens, L. Koenders, and W. Mönch, Surf. Sci. **286**, 97 (1993).
[13]C. Gu, Y. Chen, T. R. Ohno, and J. H. Weaver, Phys. Rev. B **46**, 10 197 (1992).
[14]K. Cierocki, D. Troost, L. Koenders, and W. Mönch, Surf. Sci. **264**, 23 (1992).
[15]A. B. McLean, L. J. Terminello, and F. R. McFeely, Phys. Rev. B **40**, 11 778 (1989).
[16]J. C. Patrin, Y. Z. Li, M. Chander, and J. H. Weaver, Appl. Phys. Lett. **62**, 1277 (1993).
[17]N. D. Spencer, P. J. Goddard, P. W. Davies, M. Kitson, and R. M. Lambert, J. Vac. Sci. Technol. A **1**, 1554 (1983).
[18]J. A. Stroscio, R. M. Feenstra, and A. P. Fein, J. Vac. Sci. Technol. A **5**, 838 (1987).
[19]L. J. Whitman, J. A. Stroscio, R. A. Dragoset, and R. J. Celotta, Science **251**, 1206 (1991).
[20]L. J. Whitman, J. A. Stroscio, R. A. Dragoset, and R. J. Celotta, Phys. Rev. Lett. **66**, 1338 (1991).
[21]P. Bedrossian and T. Klitsner, Phys. Rev. Lett. **68**, 646 (1992).
[22]Gu *et al.* (Ref. 13) noted that surface etching was possible when GaAs(110) was exposed to Br_2 at low temperature to form a thick layer of Br_2. Reaction was evident when the sample was warmed because Ga and As 3*d* core-level features showed 3^+ bonding configurations by 100 K. Warming to 300 K desorbed these volatile species. Such conditions of exposure are quite different from those encountered upon exposure to Br_2 at elevated temperatures.
[23]*Molecular Beam Epitaxy,* edited by H. K. V. Lotsch, Springer Series in Materials Science Vol. 7 (Springer-Verlag, New York, 1989); *Kinetics and Ordering of Growth at Surfaces,* edited by M. G. Lagally (Plenum, New York, 1990).
[24]D. K. Biegelson, R. D. Bringans, J. E. Northrup, and L.-E. Swartz, Phys. Rev. Lett. **65**, 452 (1990).
[25]K. W. Haberern and M. D. Pashley, Phys. Rev. B **41**, 3226 (1990).
[26]J. Ihm and J. D. Joannopoulos, Phys. Rev. B **26**, 4429 (1982).
[27]N. Furuhata, H. Miyamoto, A. Okamoto, and K. Ohata, J. Electron. Mater. **19**, 201 (1990).

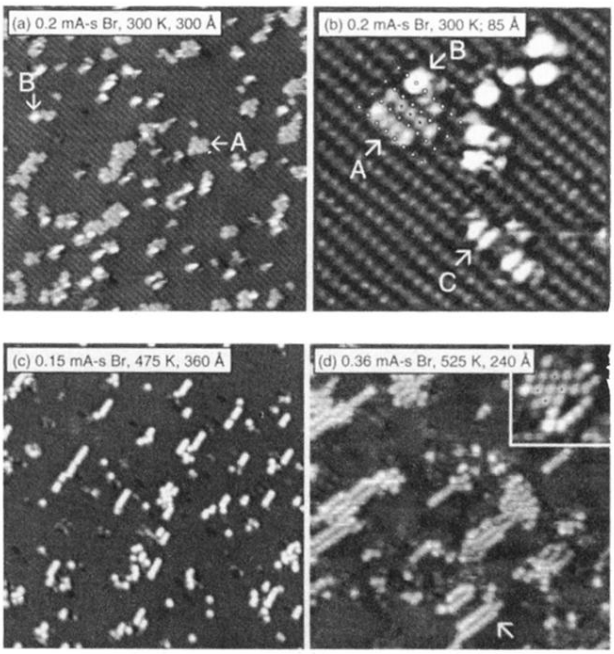

FIG. 1. (a) Adsorption structures for Br on GaAs(110) at 300 K showing A-type islands and B-type defects within the islands. (b) Curvature-enhanced image showing that the A features are localized within the rectangle formed by four As atoms. The black dots represent maxima of A-type features and the white dots represent the As atoms. The B-type features are above As atoms. (c) Image obtained after Br_2 exposure at 475 K showing linear chains elongated along [001]. (The image is not corrected for drift.) (d) Image demonstrating the coalescence of one-dimensional (1D) chains into two-dimensional (2D) islands. The arrow points to a region with (2×1) symmetry. The inset shows a region with $c(2\times2)$ symmetry as highlighted by four black dots.

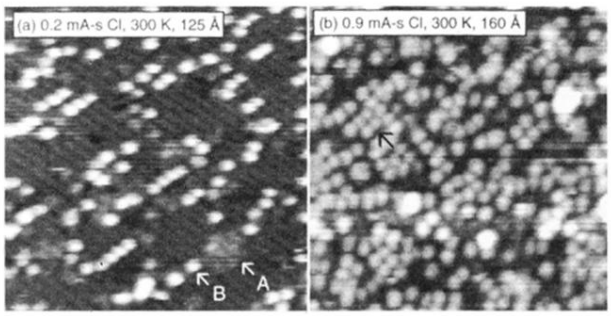

FIG. 2. (a) A 125×125-Å^2 image after a 0.2-mA s exposure to Cl_2 at 300 K showing A- and B-type adsorption features, as for Br. (b) A 160×160-Å^2 image for the nearly saturated Cl-GaAs(110) surface. The arrow highlights a B-type region with local (2×1) symmetry.

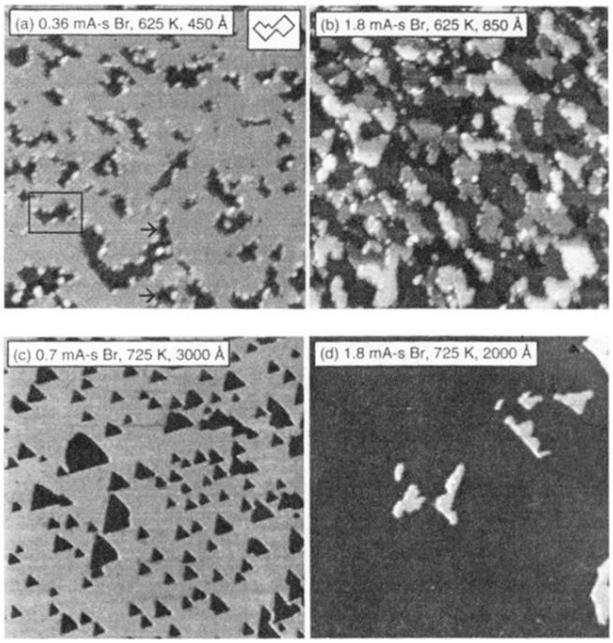

FIG. 4. (a) A 450×450-Å^2-image after exposure to 0.36 mA s of Br_2 at 625 K showing etch pits that are one layer deep and bounded by SH $[1\bar{1}0]$ and [001] steps. The inset shows the outline of the SH etch pit highlighted by the box. The arrows identify areas where second-layer pitting has occurred. (b) An 850×850-Å^2 image after a 1.8-mA s Br_2 exposure at 625 K showing five different substrate layers showing simultaneous multilayer etching. The rms surface roughness is ~2 Å. (c) A 3000×3000-Å^2 image of a typical area on an extended terrace after exposure to 0.7 mA s of Br_2 at 725 K. The image shows triangular double-layer etch pits with $\{111\}$ microfacets. (d) A 2000×2000-Å^2 image after a 1.8-mA s exposure to Br_2 at 725 K. Two layers have been removed from most of the surface. The remnants of this bilayer are evident as white islands.

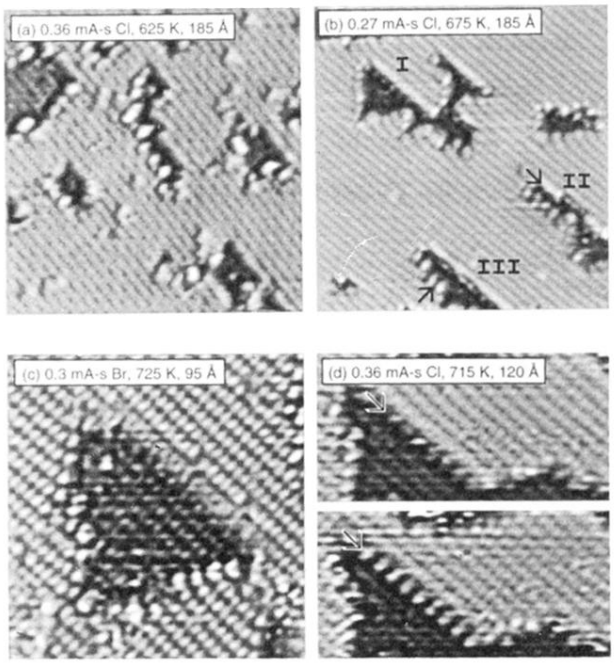

FIG. 5. (a) A 185×185-Å^2 image after Cl_2 exposure at 625 K. At this temperature, etching is initiated by SH pits composed of $[1\bar{1}0]$ and [001] steps. (b) A 185×185-Å^2 image after exposure to Cl_2 at 675 K. The etch pits are all two layers deep (4 Å) and show the onset of triangular pit formation as in I. The arrow by II points to the As-terminated $[1\bar{1}0]$-step. The arrow by III draws attention to a two-times periodicity in the step reconstruction. The reconstruction is also evident in I and II on the straight $[1\bar{1}0]$ boundaries. (c) Atomic resolution image after exposure to Br at 725 K showing a double height (DH) triangular etch pit composed of $[\bar{1}12]$, $[1\bar{1}2]$, and $[1\bar{1}0]$ steps. These DH steps form $\{111\}$ microfacets. (d) STM image obtained with negative and positive sample bias (top and bottom) after Cl_2 exposure at 715 K. The image shows a double-layer etch pit at the top and middle of the figure. The $\{111\}$ microfacet at the As-terminated [110] step has a two-times periodicity in the $[1\bar{1}0]$ direction as highlighted with an arrow for both biases.

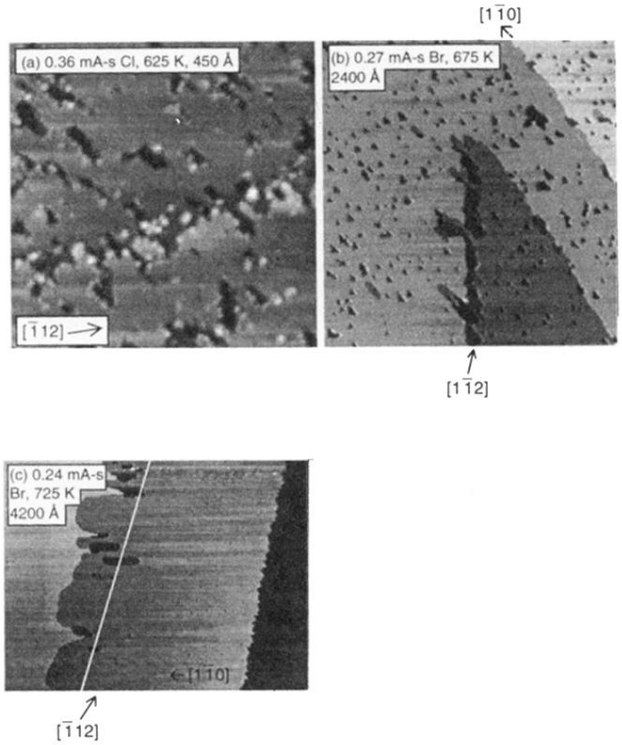

FIG. 6. (a) A 450×450-Å^2 image after Cl_2 exposure at 625 K. The image shows a [$\bar{1}$12] single-height (SH) step at the center. The etch pits on each terrace are one layer deep (2 Å) and the step shows etching along [1$\bar{1}$0]. (b) A 2400×2400-Å^2 image after Br_2 exposure at 675 K showing a [1$\bar{1}$0] step in the upper right and another that intersects a [1$\bar{1}$2] step at the center. The [1$\bar{1}$2] step has been modified substantially but the [1$\bar{1}$0] step shows little evidence of etching. (c) A 4200×3000-Å^2 image obtained after Br_2 exposure at 725 K. The white line approximates the original position of the SH step, showing retreat to the left by ~ 500 Å. The right portion of the image shows a DH step with local sawtoothlike structure. Note that the [1$\bar{1}$0] direction is along the x axis.

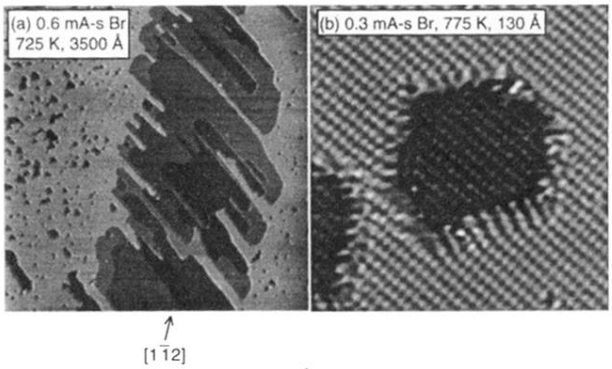

FIG. 7. (a) A 3500×3500-Å image after a Br_2 exposure at 725 K to ten times the flux of the earlier images. The left part is one layer higher than the right. The increase of Br on the surface facilitates etching into the terraces and produces multilayer exposure near the original step. (b) An atomic resolution image of a typical DH etch pit obtained after Br_2 exposure at 775 K. The etch pit is composed of six {111} microfacets.